Meteorol. Appl. 3, 5–17 (1996)

Investigating a SSM/I microwave algorithm to calibrate Meteosat infrared instantaneous rainrate estimates

V Levizzani, *Istituto FISBAT-CNR, via Gobetti 101, I-40129 Bologna, Italy*

F Porcú, *Istituto FISBAT-CNR, via Gobetti 101, I-40129 Bologna, Italy*

F S Marzano, *Dipartimento di Ingegneria Elettronica, Universitá di Roma 'La Sapienza', via Eudossiana 18, I-00184 Roma, Italy*

A Mugnai, *Istituto di Fisica dell'Atmosfera-CNR, via Galilei, I-00044 Frascati, Italy*

E A Smith, *Department of Meteorology, Florida State University, Tallahassee, FL 32306, USA*

F Prodi, *Istituto FISBAT-CNR, via Gobetti 101, I-40129 Bologna, Italy. Dipartimento di Fisica, Universitá degli Studi, via Paradiso 42, I-44100 Ferrara, Italy*

Simultaneous rainfall analyses using Special Sensor Microwave/Imager (SSM/I) passive microwave measurements and thermal infrared measurements from Meteosat are presented for two storms over northern Italy that caused damaging floods. Upwelling brightness temperatures over precipitating clouds in the mm–cm spectrum are directly associated with precipitation microphysics throughout the cloud column down into the rain layer. In contrast, brightness temperatures in the thermal infrared window, which arise from emission near cloud top, are not directly responsive to precipitation processes. However, because of the diffraction-limited nature of passive microwave detectors, microwave radiometer ground footprints are considerably larger than those characteristic of infrared sensors, even those flown at geosynchronous altitude. Furthermore, passive microwave radiometers are flown on low-earth orbiters, which produce less than ideal sampling rates, whereas optical-infrared radiometers flown on geosynchronous orbiters produce high frequency sampling concomitant with precipitation time scales. In this study, we investigate how these two types of measuring systems could be used in a complementary fashion to improve rainfall estimation. A physically based microwave algorithm is used to estimate rainfall with SSM/I measurements, whereas a two-threshold statistical technique is used for corresponding estimates from Meteosat. Results suggest that an infrared-based analysis of rainfall derived from half-hourly geosynchronous images can be improved with a calibration-transfer approach using a microwave algorithm sensitive to vertical cloud structure.

1. Introduction

Floods are the most serious natural disaster phenomenon in the countries on the northern shores of the Mediterranean (Walter, 1986). The meteorology of this region contributes significantly to hydrological hazards, with localised heavy precipitation of both frontal and convective types occurring mainly during autumn and winter, when the local circulation is driven by European and Atlantic weather systems. The complex orography and torrent-like nature of most rivers often lead to disastrous flash-floods. High-risk regions are Catalonia in north-east Spain, bordering on France and the Mediterranean, Provence–Côte d'Azur in south-east France, bordering on Italy and the Mediterranean, and Italy, where the orography, the high population density and the location of buildings in scanty plain areas increase the risk of extensive damage and casualties (Siccardi, 1987). Flooding on Italy's west coast, which is exposed to Atlantic weather systems, is

particularly hazardous. Of note are the regions of Liguria on the north-west coast bordering France, Tuscany, especially the Arno river basin crossing Florence, and the mountainous areas such as Calabria in continental southern Italy. The most notable recent destructive floods were:

(a) The 1966 Arno river flood in Florence, a disaster which caused extensive damage to Italy's Renaissance cultural heritage.
(b) The 1987 events in the Valtellina area, involving flash floods and landslides on the southern slopes of the Alps.
(c) The 1992 and 1993 events in Liguria, involving flash floods and casualties.
(d) The destructive 1994 floods in the Piedmont area, involving over 60 casualties, extensive property damage, and dislocation.

These disasters have wrought enormous social and economic havoc. Therefore, any improvements in monitoring, forecasting, and warning systems that can mitigate even a part of their impact deserve attention (see Barrett & Michell, 1991).

The nowcasting of extreme flood events is based on modelling the runoff of the basins, which is possible only if hydrologists are provided with the necessary meteorological inputs, particularly precipitation intensity at precise locations. An ideal nowcasting system would include a dedicated numerical model and specialised data support networks. These involve conventional surface and upper-air meteorological stations, a radar network, a dense mesonet, and a continuous stream of satellite data inputs. Radar measurements would be particularly helpful in defining the internal structure of precipitation systems and estimating precipitation rates. Besides their use for precipitation retrieval, satellite observations can provide additional information on storm evolution, particularly an overall picture of the larger-scale weather pattern responsible for the precipitation. A single radar, not integrated into a network, would be of limited value for a flood warning system over the northern Mediterranean coast because the systems often move rapidly and beyond the range of a single radar during critical stages of basin saturation. In fact, for certain meteorological situations and locations, even a radar network would not be sufficient for obtaining the accurate precipitation measurements needed for issuing timely flood warnings. Moreover, the generally complex terrain and the confined nature of many of the flood-prone watersheds often make it difficult for radars to obtain clutter-free measurements. The northern coast of Italy is notable in this regard.

Dedicated numerical models can be used to ensure timely warnings, although they require an observational support system which is not generally available (for example, comprehensive radar and mesonet networks). Satellite measurements can be used to overcome a number of the problems associated with precipitation monitoring and obtaining spatial fields of precipitation intensity appropriate for basin runoff models, though satellite measurements are by no means free of difficulty. For the type of high spatial scales intrinsic to the watersheds of the northern Italian coast, satellite measurements suffer from ground resolution (with polar orbiters generally superior to geosynchronous ones) and time sampling problems (with geosynchronous orbiters far better than polar ones). There is the added difficulty of having to convert the radiation signals into precipitation estimates, which is a non-trivial and elusive retrieval problem given that today's sensors were never really optimised for precipitation measurement. Satellite sensors, on the other hand, are ideal for monitoring large areas uniformly and for pinpointing severe weather systems in their entirety, key capabilities generally lacking in other observational networks. It is also worthwhile pursuing improved precipitation estimation methods from satellites for inputting into nowcasting and flood warning systems by taking advantage of the respective strengths of the different sensors and orbit configurations.

To date, flood forecasting systems designed for the Mediterranean area consist of rainfall-runoff models which must use incomplete and imprecise average rainrate information derived from sparsely distributed raingauges located within individual sub-catchments. As a result, runoff models often fail, not because of problems with the models, but because of problems with the inputs. The spatial non-uniformity of rainfall and rapid storm movement suggest a warning system based on radar monitoring and the implementation of distributed models. However, the current radars in Italy are not configured into a network, their data are not generally available for research, and their operation is supervised by local government authorities who cannot guarantee continuous surveillance or provide coordinated surveillance strategies for operational forecasting. The latter situation is particularly unfortunate since hazardous storms do not recognise or acknowledge political boundaries. This situation motivates an investigation of means to improve the accuracy of time-sequenced rainrates obtainable from geosynchronous infrared measurements.

Two heavy rainfall events over northern Italy were investigated. Both caused flash flooding, extensive property damage, and numerous casualties. The events took place on 23 August 1987 and 27 September 1992, referred to respectively as the Val Brembana flood (in the Valtellina region of the Italian Alps) and the Genoa flood on the Tyrrhenian coast. The *Special Sensor Microwave/Imager* (SSM/I) microwave (MW) rain profile algorithm of Marzano *et al.* (1994) and the infrared (IR) rainmap algorithm of Negri *et al.* (1984), configured for Meteosat, are used for the analysis. A

preliminary study of the first event was performed using two different versions of both algorithms to test the feasibility of using the MW algorithm to calibrate the IR algorithm better (see Levizzani *et al.*, 1993). Both events were selected, along with 26 other events distributed over the globe, as test cases for the second phase of the NASA WetNet *Precipitation Algorithm Intercomparison Project* (PIP-2) (see Smith *et al.*, 1995). The objective of PIP-2 is to use SSM/I case studies of a variety of storm events at the instantaneous pixel-scale, along with coincident radar and/or rain-gauge measurements, to help improve the physical basis of a large group of SSM/I precipitation retrieval algorithms.

This study is the first to use microwave and infrared retrieval techniques together to monitor extreme flood events in Italy for application to satellite-based nowcasting. In so doing, we are examining whether satellite remote sensing can provide a comprehensive and routine means of monitoring hazardous rainfall events, and evaluating whether such techniques can help identify where rainfall events are likely to become extreme.

2. Satellite platforms and rain estimation algorithms

The SSM/I on board the spacecrafts of the USAF *Defense Meteorological Satellite Program* (DMSP) has led to a major breakthrough in satellite-based precipitation measurement (Wilheit, 1986; Spencer *et al.*, 1989). This scanning-type instrument measures MW radiation over a 1400-km wide swath at four separate frequencies, 19.35, 22.235, 37.0 and 85.5 GHz, the latter extending the spectral range of previous instruments into the strong scattering regime (with regard to precipitation-size particles). The radiometer operates in dual polarisation (both vertical and horizontal) at each frequency except the water vapour channel at 22.235 GHz, where only vertical polarisation is measured. The effective ground resolutions at these different frequencies are approximately 69×43, 60×40, 37×28 and 15×13 km^2 (in order of lowest to highest frequency). Infrared images (10.5–12.5 μm) from the *Visible and Infrared Spin Scan Radiometer* (VISSR) of the European Space Agency's Meteosat satellite program can also be used for precipitation retrieval based on the general relationship between 'cold' cloud area and rainfall. The Meteosat IR channel ground resolution is approximately 5×7.5 km^2 over northern Italy, with an image repetition period of 30 minutes. The VISSR scans these latitudes at approximately the 21st and 51st minute of each hour. We acquired this type of Meteosat image sequence for the two events under study.

Mugnai *et al.* (1990) addressed the important question of where MW radiation originates and from which atmospheric layers different frequencies sense radiation in a precipitating cloud. This study was based on the use of a limited-area model configured for resolving explicit cloud systems to describe the thermodynamic structure of the cloud and the horizontal and vertical distribution of cloud hydrometeors (Tripoli, 1992). A high-resolution, multiple-scattering radiative transfer model was applied at the SSM/I frequencies to determine the effect of various categories of liquid and frozen hydrometeors on upwelling brightness temperatures measured at satellite altitude. Since that study, a number of SSM/I retrieval algorithms have been published which base the cloud microphysics on cloud model simulations, and which are designed to retrieve vertical rain structure. In addition to the Marzano *et al.* (1994) algorithm used for this investigation, algorithms have been published by Kummerow & Giglio (1994), Smith *et al.* (1994), Evans *et al.* (1995), and Pierdicca *et al.* (1996).

Negri *et al.* (1984) developed the *Negri–Adler–Wetzel Technique* (NAWT), a computationally efficient rainfall estimation method based entirely on IR measurements from geosynchronous satellites, with potential for operational monitoring and forecasting (Levizzani *et al.*, 1990). The application of the technique, which was originally developed and tested for tropical convection, to mid latitude precipitation systems is by no means without difficulty. Using Meteosat measurements, Levizzani *et al.* (1990) and Marrocu *et al.* (1993) reported that the best performance of the NAWT at mid latitudes is obtained for averaged rainfall estimates at suitable space–time intervals.

The advantage of passive MW measurements over IR measurements is that they are directly responsive to precipitation microphysics. However, because the MW measurements are diffraction limited, and thus ground resolutions are relatively low, and because the sensors have only been flown on low orbiting satellites (due to ground-resolution constraints), the measuring capacity of MW radiometers does not properly address the fundamental space–time scales of precipitation. Conversely, IR sensors on board geosynchronous satellites, which measure thermal radiation largely emitted by cloud tops, provide little meaningful signal on microphysical structure. Yet, given the much higher ground resolution and the time sequencing offered by geosynchronous platforms, IR measurements make it possible to follow storm development at the relevant space and time scales. Thus, there is a natural basis for combining the two types of measurement and taking advantage of their respective strengths. Adler *et al.* (1993) tested this idea by combining SSM/I and GMS (the Japanese Geostationary Meteorological Satellite) measurements for rainfall estimates over Japan, the aim being to obtain mean monthly values for climate studies. The present study combines SSM/I and Meteosat measurements to take advantage of their complementary information on the instantaneous precipitation process, a basic requirement for nowcasting.

3. Description of events

3.1. Meteorological conditions

The surface chart at 1200 UTC on 23 August 1987 is shown in Figure 1. Conditions which generally lead to the development of thunderstorms in northern Italy were already present. A cold front was approaching from the north-west in conjunction with a widespread low-pressure system dominating the Mediterranean. The anticyclone (often referred to as the 'Azores anticyclone' due to the proximity of its center to the Azores islands) which normally dominates the Mediterranean region at this time of year had weakened, no longer acting as a barrier to cold north Atlantic air masses that could then penetrate to lower latitudes. At this time Cu and Sc clouds formed along the leading edge of the cold front above the Pyrenees mountains and Iberian coast. Six hours later, as the front reached south-east France (Provence–Côte d'Azur) and north-west Italy, warm air from the Mediterranean and Po river valley was lifted against the Alps and a line of thunderstorms developed along the front. The strength of the low-pressure system and the south-west circulation at upper levels (not shown) continuously fed warm, humid air into the thunderstorms, causing heavy and long-lasting precipitation. Flooding occurred in south-east France, causing extensive damage, casualties and virtually paralysing the area for some days. In Italy a thunderstorm hit Val Brembana and Valtellina (some 70 km north-east of Milan) in the Alps, the heavy rainfall causing flash flooding and landslides over a primarily agricultural and tourist region.

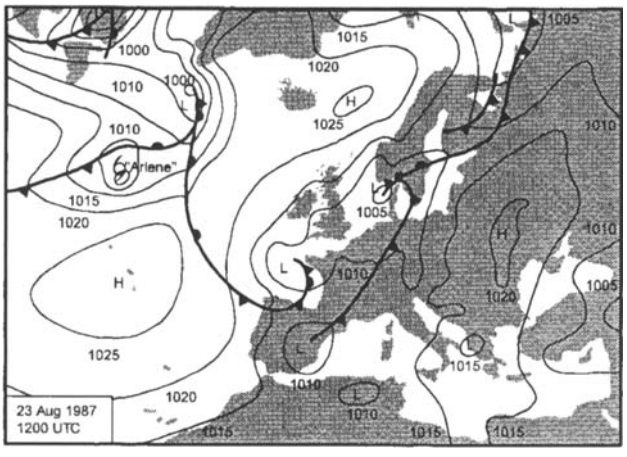

Figure 1. *Surface weather map at 1200 UTC for 23 August 1987.*

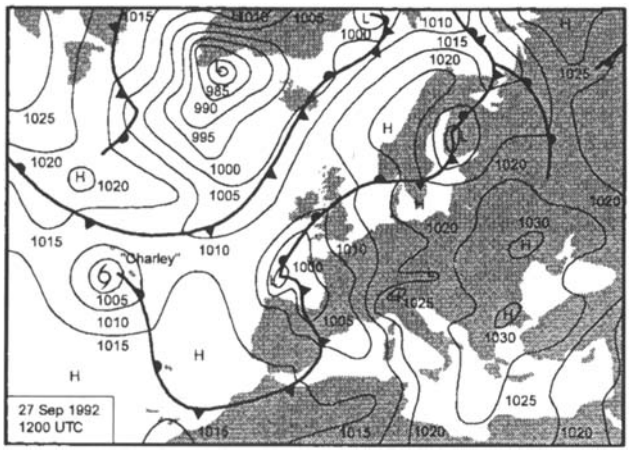

Figure 2. *Same as Figure 1 but for 27 September 1992.*

The meteorological situation of 27 September 1992 developed out of Mediterranean region surface and upper-level circulations typical of the latter part of the month (the surface chart at 1200 UTC is shown in Figure 2). On 23 September the cyclonic circulation extending from Central Europe to Spain propagated eastward, gradually influencing northern Italy. During the last week of September, upper-level flow over northern Italy included a prevailing unstable meridional component. At the same time, the summer anticyclone started to weaken, allowing the central European depression to expand towards the Mediterranean. A period of generally unstable weather followed, with two slow-moving Atlantic frontal systems containing thunderstorms reaching northern Italy. The first thunderstorm hit the west coast of Liguria and south-east France, while the second hit the city of Genoa and its environs. This situation is not that unusual at this time of the year, when the relatively stable summertime conditions of the Mediterranean basin break up and winter meteorology becomes established. Our focus is on the Genoa event because SSM/I coverage was available.

On 25 September at 1200 UTC a large depression formed over the North Sea down to the Bay of Biscay, with an associated frontal system rapidly moving eastward. At 0000 UTC on 26 September pressures over the Bay of Biscay dropped significantly, the depression extending to Spain and the Atlantic coast of France. At the same time a new pressure minimum developed between the Balearic Islands and North Africa. By 1200 UTC the two depressions had merged and a low pressure ridge formed extending to North Africa. The frontal system was then able to travel towards Italy from the south-west. By 0000 UTC on 27 September the cold front had reached the Pyrenees curving down to Morocco. Its approach speed was high because of the strong upper-level south-west winds; by 1200 UTC it had reached the Gulf of Lyons. At the same time a warm and humid surface air current from the southern Mediterranean and North Africa was blowing over the Côte d'Azur, Provence and Liguria. Given the large-scale differential advection and associated rapid vertical lifting of warm humid air ahead of the front, thunderstorms were imminent. A violent pre-frontal storm hit the Genoa area in the late morning and early afternoon of 27 September, causing flash flooding.

3.2. Satellite observations

The top-left panel of Figure 3 shows an SSM/I brightness temperature (T_B) image at 85.5 GHz (vertically

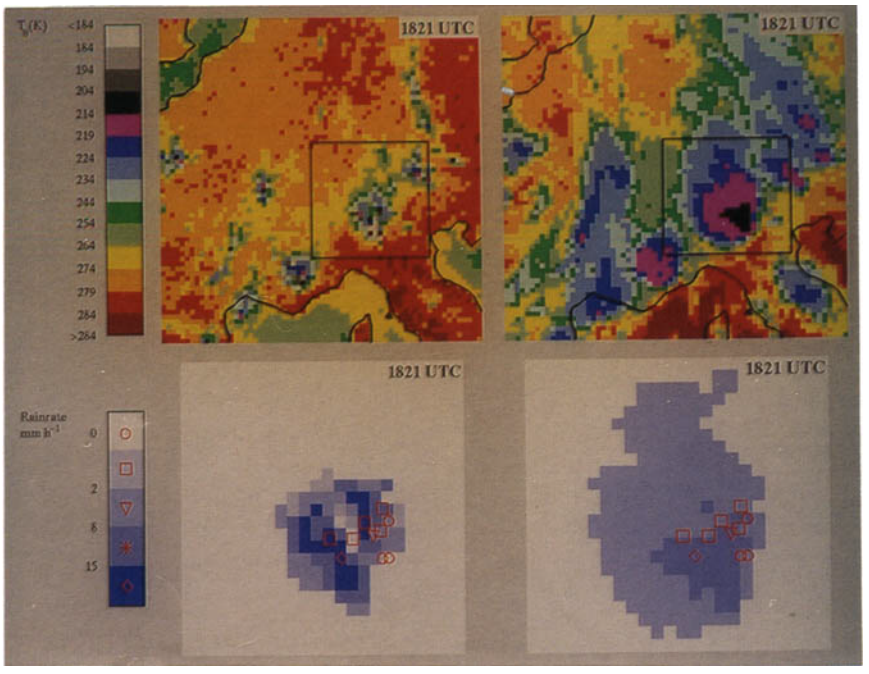

Figure 3. *Comparison of rainfall estimates using the 1821 UTC SSM/I overpass and Meteosat IR image for the 23 August 1987 event. The top panels show the SSM/I 85.5 GHz vertically polarised image (left) and the corresponding Meteosat 11.5 μm image (right). The bottom-left panel shows the SSM/I-based rainfall estimate using the IFA-SAP algorithm, and the bottom-right panel shows the Meteosat-based estimate using the NAWT algorithm. The bottom panels represent enlarged views of the areas delimited by the black squares in the top panels. Raingauge measurements are superimposed (red symbols). The images are displayed in Mercator projection.*

polarised) for the 23 August 1987 event during the descending pass over northern Italy at 1821 UTC. Attention is focused on the largest storm of the major cloud system enveloping a complex of convective storm cells along the cold front (green–blue to white area straddling the Swiss–Italian border in the upper-central part of the image). The white-to-black pockets within the storm ($T_B \leq 214$ K) are associated with the most intense cells, in which large ice particles inhibit the upwelling radiation emitted from lower cloud and rain layers from reaching the radiometer. In general, backscattering from large drops and ice particles is the physical mechanism responsible for the general appearance of the storm as a cold feature over a warmer continental background. Yellow-to-red pixels ($T_B \geq 264$ K) represent either cloud-free areas over land/sea, or regions where clouds are transparent at 85.5 GHz. The pixels immediately surrounding the storm cells (green, blue, cyan and magenta) are non-precipitating areas and/or high-level cirrus clouds. The Meteosat IR image at 1821 UTC is shown in the top-right panel of Figure 3. Green-to-black pixels ($204 \leq T_B \leq 264$ K) along the cold front represent cloud-top temperatures of the storm cells. No inference can be made on the storm's internal structure at this wavelength. Yellow-to-red pixels ($T_B \geq 264$ K) indicate low-level cloud and cloud-free areas. The bottom two panels in Figure 3 (and the following figure) are the actual rainrate retrievals from the MW and IR algorithms; these results are discussed in section 5.

Figure 4 (top-left panel) shows the 85.5 GHz SSM/I image at 1555 UTC on 27 September. Three envelopes of low brightness temperature are present: (a) an area in central Italy over Tuscany and the coast of the Tyrrhenian Sea almost down to Rome; (b) a relatively small area in south-east France; and (c) the area of interest extending from the Ligurian coast inland to Genoa and north-west Italy. The corresponding Meteosat IR image at 1551 UTC is shown in the top-right panel.

By comparing the IR images with the corresponding MW images for both cases the following features can be noted:

(a) The region of low brightness temperature around the core of the thunderstorms is more extensive in the Meteosat IR images because IR radiation is highly affected by the presence of thin clouds, whereas MW radiation is not.
(b) The Meteosat IR images are smoother and exhibit less detail than the corresponding SSM/I MW images. IR brightness temperatures do not fall below 200 K, while at 85.5 GHz, backscattering from large particles reduces brightness temperatures less than 120 K. This stems from IR frequencies responding only to cloud-top radiation, while MW frequencies respond to microphysical processes emanating from within the cloud.

A sequence of Meteosat IR imagery from 1351 to 1851 UTC on 27 September is shown in Figure 5 to illustrate the evolution of the 1992 storms. At 1351 UTC, two cold areas (black and magenta) over Liguria and Tuscany correspond to the two pre-frontal storms which remained over the area for many hours, causing

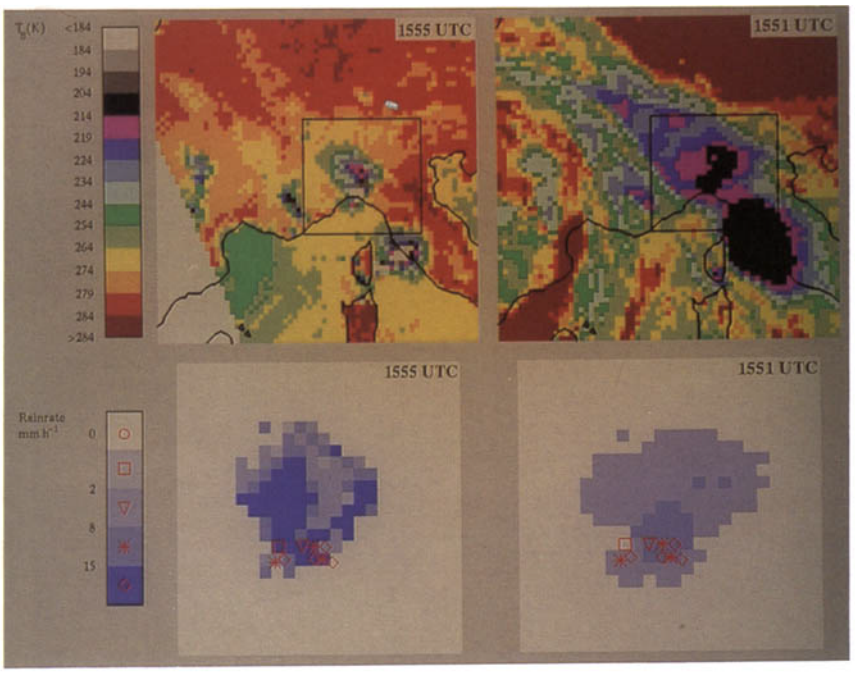

Figure 4. *Same as Figure 3 but at 1555 UTC for the 27 September 1992 event.*

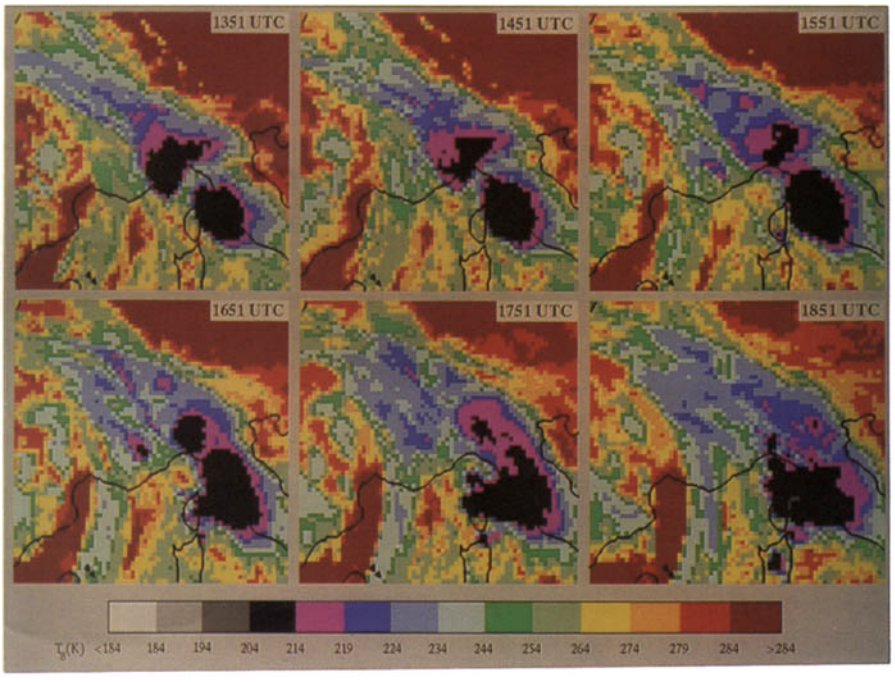

Figure 5. *Meteosat IR image sequence from 1351 to 1851 UTC for the 27 September 1992 event.*

heavy precipitation in the mountainous coastal area of Liguria. The storms then merged and precipitation rates over Liguria gradually decreased. Inspection of the IR imagery reveals the potential for danger, manifested by the slow moving frontal passage over the city of Genoa. The storm, continuously fed by warm prefrontal air and persisting for many hours, eventually led to flooding conditions. It is monitoring these aspects of the storm, i.e. the system's evolution and flood hazard potential, that makes the Meteosat data so vital.

It is helpful to understand the degree of correlation between the SSM/I and Meteosat measurements. The scattering index (SI) introduced by Grody (1991), which embodies both high and low frequency SSM/I measurements and is designed to identify both cloud and background scattering surfaces, has been chosen as a means to compare the SSM/I multi-frequency measurements against the Meteosat IR temperatures. In essence, as the SI index increases, the degree of scattering increases, which for a raining cloud is indicative of higher rainrates. Coincident SSM/I and Meteosat overpasses for the Val Brembana and Genoa events are compared within the SSM/I rain area by simply plotting the SSM/I-derived SIs against the Meteosat-

derived IR temperatures taken as averages over the SSM/I ground footprints. The IR temperature dynamic range for 23 August 1987 in Figure 6(*a*) is around 10 K over 125 units of SI. Although the scatter is large, there is detectable positive correlation indicated by the linear regression line. The scatter diagram for 27 September 1992 in Figure 6(*b*) shows a dynamic range of 20 K over the same SI interval, also with substantial scatter, but with basic underlying correlation (although clearly not linear). Therefore, even though the rms differences between the MW and IR quantities are significant, the non-zero slopes in the relationships suggest that the two measures can be intercalibrated.

Rainfall measurements from raingauges were available for small areas in both cases and are thus used for comparison with the satellite rain estimates. However, meaningful quantitative verification of rainrate retrievals from either the IR or MW algorithms using raingauge measurements is very problematic because of the highly different spatial and temporal integrations intrinsic to the two types of measurements. Therefore, little emphasis can be given to such comparisons, and by no means should the raingauge comparisons be taken in the context of a calibration procedure.

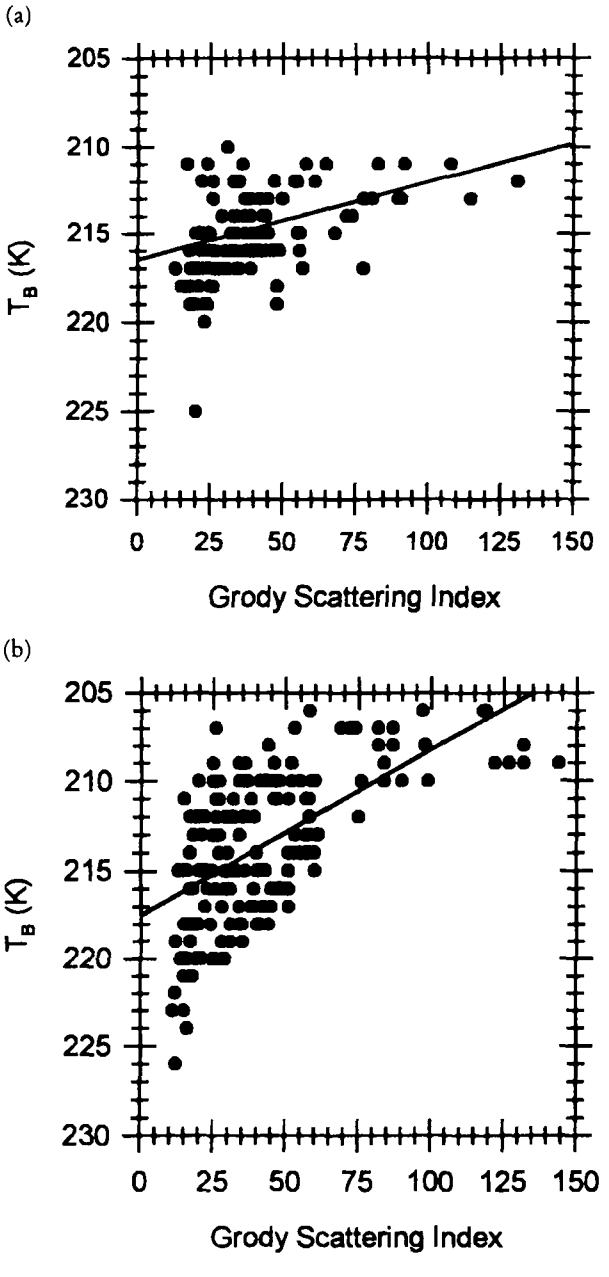

Figure 6. *Scatter diagram between Meteosat's brightness temperature (ordinate) and Grody's SSM/I scattering index (abscissa): (a) 23 August 1987; (b) 27 September 1992.*

4. Description of MW and IR algorithms

A physically-based precipitation profile retrieval algorithm using SSM/I measurements as input was proposed by Smith *et al.* (1992) and Mugnai *et al.* (1993); this algorithm is described in detail by Smith *et al.* (1994). Using the same microphysical approach, Marzano *et al.* (1994) developed an alternate inversion scheme to replace iterative radiative transfer (RTE) calculations with statistical calculations applied to basis functions linking microphysical structures to multifrequency brightness temperature vectors. The exact relationships between the microphysics and brightness temperatures were obtained through RTE calculations. The resultant algorithm has many of the same physical attributes but provides a more computationally efficient means to carry out the inversion process. Its major features are:

(a) It is based on physical inversion and is therefore flexible to improvements of the embedded physical and numerical techniques.
(b) An explicit cloud-mesoscale model is used for generating the microphysical underpinnings, an approach that allows tuning of the microphysics according to specific cloud environments through appropriate simulations.
(c) Besides surface rainrates, concentration profiles of various hydrometeor categories are generated and consistent with the individual channel brightness temperatures.
(d) It accounts for the fact that surface rainrates are only indirectly related to the upwelling microwave radiation at the top of the atmosphere; rainrates are physically derived through a fallout equation based on the profiles of precipitating liquid and ice hydrometeors.
(e) Variance information associated with a given retrieval is evaluated, which helps in probability forecasting and in understanding uncertainty.

The algorithm, hereafter referred to as IFA-SAP (after the Institute of Atmospheric Physics of the Italian National Council of Research at Frascati and the University of Rome 'La Sapienza'), has already been applied to spaceborne and airborne passive microwave radiometer data (Allam *et al.*, 1993, and Marzano *et al.*, 1994) and to the two storm data sets used in the present study.

The application of a microwave algorithm over a land background is not without its difficulties, which are mostly related to detection of rain through some type of 'screening' procedure prior to the actual conversion of a brightness temperature vector to rainrate. Although in earlier years, precipitation estimation over land was generally thought to be untenable, with the advent of the high frequency 85.5 GHz channels on SSM/I, which are sensitive to precipitation-induced scattering, land-based retrieval algorithms are now commonplace; see the algorithm reviews in Allam *et al.* (1993), Wilheit *et al.* (1994), and Smith *et al.* (1995). The studies of Spencer *et al.* (1989), Smith & Mugnai (1989), Mugnai *et al.* (1990), and Ferraro *et al.* (1994) have addressed the issue of precipitation contrast over a land background, and have shown through observations and modelling calculations that depending on the nature of the ice content in a column, rain is detectable and quantifiable. Notably, of the 20 algorithms submitted to the PIP-2 project, 15 are capable of retrieving rainrates over a land background. The review of Petty (1995) on the subject of satellite-based rainfall estimation over land is a useful overview on this subject.

For purposes of this study, the 85.5 GHz polarisation-corrected temperature (PCT) approach of Spencer *et al.* (1989) has been used to 'screen' the microwave T_Bs for the presence of rain. This is a straightforward discriminant test that determines relative to a fixed threshold whether the cloud column has generated enough scattering-induced depolarisation to qualify the cloud as a raining event. It is important to recognise that rain detection and rainrate (RR) estimation are distinct elements of almost all current SSM/I precipitation algorithms, particularly multi-channel algorithms applied to land surfaces (Smith *et al.*, 1995). The nomenclature for discriminating these two processes consists of the terms 'screening' and T_B–RR conversion. The reason for separating these two processes stems from the fact that there are a variety of discriminant-type tests that are used for making binary classifications of brightness temperature vectors into rain or no rain categories, which contain physically or empirically based relationships that are not used in converting T_Bs into rainrates on a continuous scale. Another way of saying this is that the independent variables of a T_B–RR conversion scheme (whether it be a statistical regression, a physically based functional transform, or a RTE model-based inversion process), are not the same variables that are useful in refined screening procedures. Moreover, most T_B–RR conversion schemes will transform brightness temperature vectors associated with the land background into positive rainrates either deterministically or probabilistically, simply because there are no inherent limits in the conversion relationships related to rain–no-rain radiative thresholds.

Discriminant functions used in 'screening' procedures generally consist of up to four types of test threshold:

(a) A low frequency (e.g. 19.35 GHz) emission threshold denoting a minimum detectable rainrate signature produced by the liquid rain layer.
(b) A high frequency (e.g. 85.5 GHz) scattering threshold denoting a minimal degree of T_B depression induced by large ice (and possibly rain) particles characteristic of a raining cloud.
(c) A polarisation or depolarisation threshold (appropriate at all frequencies) denoting the likely separation between the mostly polarised land surface and the mostly unpolarised rain column.
(d) A dual-frequency T_B difference threshold denoting the distinct cross-spectral difference signatures of a land surface and rain layer.

In the original NAWT algorithm, cloud area (A_C) was identified by the 253 K isotherm, with isotherms $T_{50\%}$ and $T_{10\%}$ defining the 50% and 10% coldest portions of the cloud area, respectively. Assuming that rain volume (R_V) is directly proportional to A_C, the authors assigned the following rainrate (RR) thresholds for the FACE thunderstorms: RR = 8 mm h^{-1} for $T_B < T_{10\%}$, RR = 2 mm h^{-1} for $T_{10\%} < T_B < T_{50\%}$, and RR = 0 for $T_B > T_{50\%}$. These rainrates are independent of cloud life history and are referenced to convective rain clouds from decaying cumulonimbus over Florida, which have lifetimes of 1 to 3 hours. The application of the NAWT algorithm to situations other than tropical thunderstorms is expected to give worse results, since the physics of the rainfall process is often different (Levizzani *et al.*, 1990).

Rainrate assignments can be changed and temperature thresholds varied according to the intrinsic thermodynamic stability, background cloud condensation nuclei concentrations, topography, terrain height and the general nature of the local synoptic flow regimes. For the present study, the NAWT algorithm was modified in the initial determination of cloud area A_C. The 1987 and 1992 thunderstorms of this study were frontal and pre-frontal mid-latitude convective storms embedded in stratiform cloud environments. If the NAWT algorithm were to be applied in its original form, the cloud area A_C would be overestimated and would partially include stratiform non-precipitating clouds surrounding the convective precipitating core and anvil with temperatures lower than 253 K. For the case of a single mature tropical thunderstorm, the NAWT algorithm discriminates between precipitating and non-precipitating portions of cloud area A_C; even for merged thunderstorms it can perform correctly. Problems arise, however, when thunderstorms are embedded within a cold stratiform cloud system, dynamically and microphysically independent of the storm's convective development. This is exactly the case for both our events and for many heavy-precipitating frontal convective systems at mid latitudes. Negri & Adler (1993) lowered the cloud area threshold to 235 K for their intercomparison of satellite rainfall estimation techniques over Japan to agree

more closely with regions of scattering in the 85.5 GHz SSM/I measurements, and adopted an empirical discrimination threshold between raining and non-raining clouds. The 235 K isotherm is equivalent to that used for rain area thresholding by Arkin & Meisner (1987) and adopted for the NOAA GPI technique (Arkin & Janowiak, 1991).

For this application, the convective storms were isolated from the environment by means of a temperature gradient that took into account the horizontal structure of the cloud top by following two basic criteria:

(a) High values of the horizontal temperature gradient (<10 K per pixel) were assumed to delimit the convective cloud.
(b) An inversion of the gradient separates two adjacent convective areas.

In the Genoa case, for example, the NAWT alone would consider the Genoa and Tuscany storms as a single cloud with obvious consequences on the assignment of the 50% and 10% coldest areas. The gradient method allows for a separation of the two storms, which is confirmed by the time sequence in Figure 5.

5. Algorithm results and discussion

The rainfall retrievals and raingauge measurements are shown in the bottom panels of Figures 3 and 4 for the 1987 and 1992 events, respectively. The salient features of these diagrams can be summarised as follows.

(a) Qualitative similarity is found between the SSM/I rain areas and the corresponding Meteosat rain areas, with an important difference between the two cases. For the 1987 event, the similarity is between the SSM/I-derived precipitation area and the Meteosat's high-rainrate area, whereas for the 1992 storm, the similarity is with respect to the overall rain area found by Meteosat. As ambiguous as this may appear at first sight, the existence of rain area similarity for both cases at the different NAWT thresholds provides an incentive for recalibrating the NAWT thresholds to achieve consistency between the instantaneous Meteosat retrievals and the SSM/I retrievals. Note that although the two storms had quite different morphologies and therefore different structures (see section 3), the microphysical database used in the IFA-SAP MW algorithm was the same for both cases. This aspect of the MW algorithm can be improved, and is now in progress based on a new mesoscale model simulation of the 1992 Genoa storm event (Smith *et al.*, 1996) using the Tripoli (1992) limited-area non-hydrostatic model.
(b) The IR algorithm generally tends to overestimate the precipitation area as compared with the SSM/I algorithm because it uses only cloud-top temperatures regardless of the internal structure. Even after the modification introduced in section 4, cold non-precipitating clouds still contribute to the definition of rain area.
(c) In some cases the IR algorithm estimates zero rainrates inside SSM/I precipitation areas, which is a questionable feature of a combined algorithm, but which is probably related to differing spatial resolutions.
(d) The SSM/I estimates exhibit greater detail than those of Meteosat. This is due to the direct link between the MW measurements and the internal cloud microphysics.
(e) Based on the comparison between satellite retrievals and raingauge measurements, a raingauge-based absolute calibration procedure cannot be justified.

As to the final point, the space and time integration factors applicable to the satellite and ground instruments (given the storms' positioning over mountainous terrain) are so different that direct comparison can only be qualitative. In essence, the SSM/I measurements provide estimates over areas of about 200 km^2, while raingauge measurements are representative only of point sites. The scatter diagrams of rainrates calculated by the IFA-SAP algorithm versus the raingauge measurements for the 1987 and 1992 events are shown in Figure 7. They discriminate between SSM/I pixels lying within the NAWT algorithm's low- and high-rainrate areas. For the 1987 event, the SSM/I and raingauge measurements are totally uncorrelated. For the 1992 event, correlation is better but weak. For the 1987 event, the raingauge measurements can only be used qualitatively since landslides destroyed many of the gauges during the course of the storm and during a previous severe flood-producing storm that occurred approximately one month earlier (July 28). The prior event produced 230 mm of rain in three days. For the 1992 event, the comparison results are more encouraging, although the raingauges report larger maximum rainrates (about 40 mm h^{-1}) because they sample a much smaller volume than the SSM/I field of view.

Figure 8 shows the histograms of the number of SSM/I-derived estimates versus rainrate within the NAWT algorithm's rain area for both the Val Brembana and Genoa events. The histograms show that rainrate properties were different for the two cases, somewhat uniformly distributed between 0 and 22 mm h^{-1} in 1987 but bi-modally distributed with definite peaks at 4 and 18 mm h^{-1} in 1992. The latter case also exhibits a larger average precipitation rate. The bi-modality in rainrate distribution indicates that the structure of the Genoa storm is similar to the ideal NAWT storm, i.e., a high rainrate convective core and a lower rainrate stratiform anvil.

Figure 9 shows the number of SSM/I pixels within Meteosat's low- and high-rainrate areas for the Val Brembana event versus the rainrate estimated by the

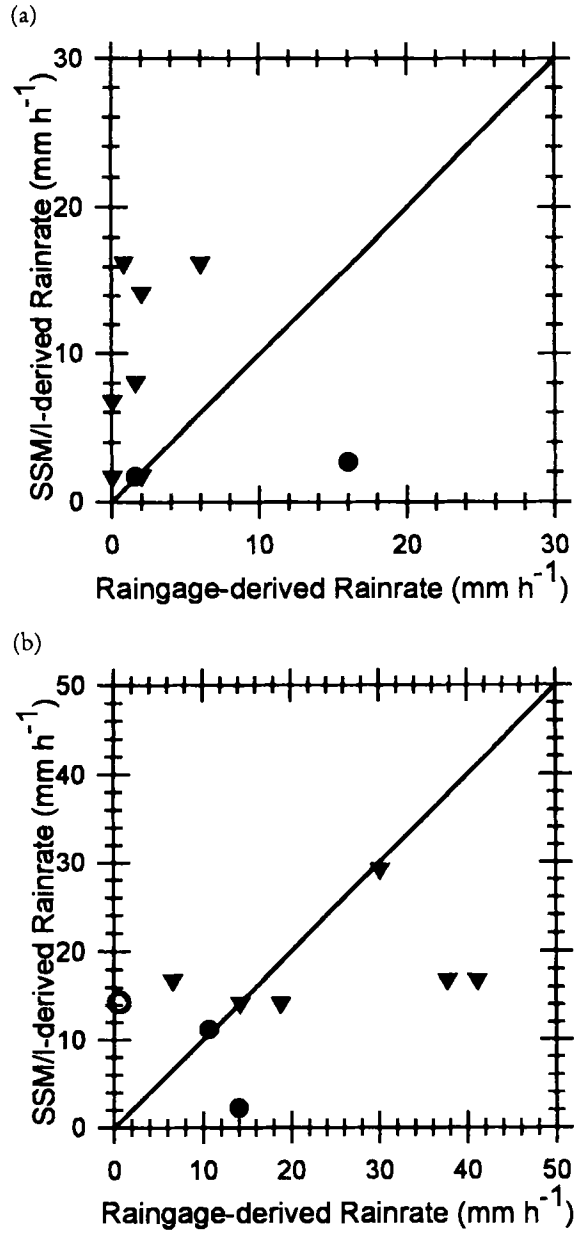

Figure 7. *Scatter diagrams of SSM/I-derived rainrates versus raingauge-measured rainrates for the two events: (a) 23 August 1987; (b) 27 September 1992. The symbols identify the Meteosat rainfall category to which the SSM/I and raingauge data belong: 0 mm h^{-1} (hollow circle), 2 mm h^{-1} (filled circle), and 8 mm h^{-1} (filled triangle).*

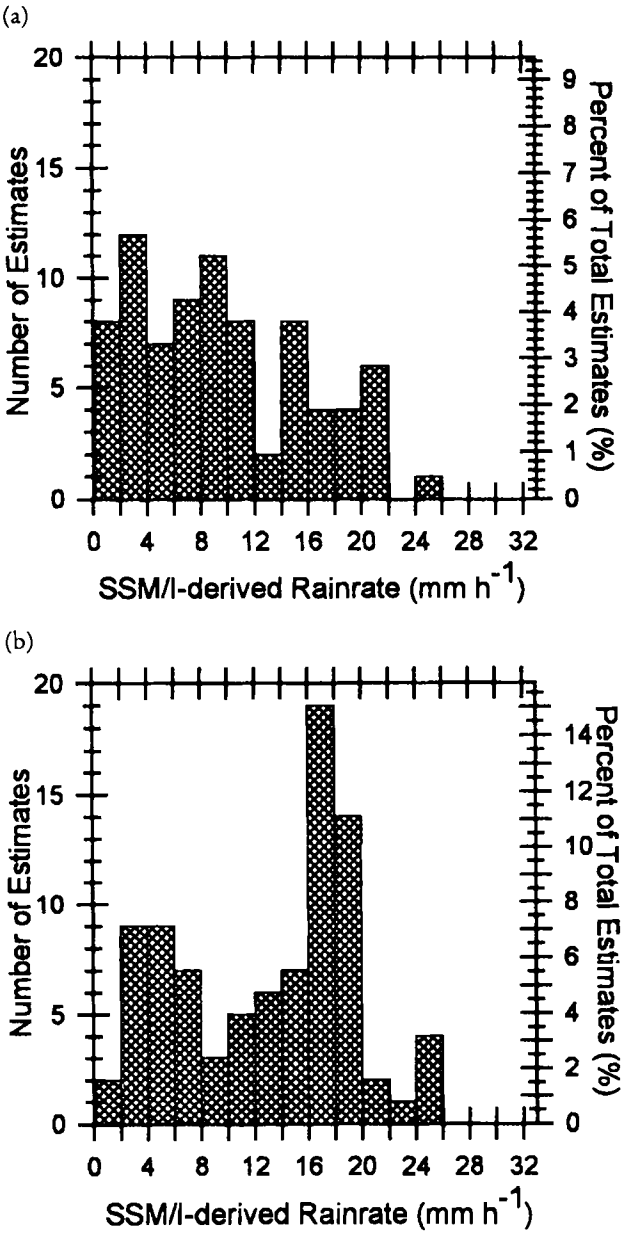

Figure 8. *Histograms of SSM/I-derived rainrate distribution for the two events within Meteosat rain areas: (a) 23 August 1987; (b) 27 September 1992. Percentage values refer to the entire Meteosat-based precipitating area.*

IFA-SAP algorithm. Figure 10 shows the same result for the Genoa event. There is a relatively wide range of SSM/I rainrates, with nearly the same maximum value regardless of whether the pixels are selected for the low- or high-rainrate areas. However, Table 1 shows that the average rainrates from the MW estimates are considerably larger than the IR estimates within the NAWT algorithm's high-rainrate areas. Moreover, for the 1992 Genoa storm, the average MW estimate for the low-rainrate area is considerably larger than the IR estimate. Basically, for the two events, only the corresponding MW and IR estimates for the low-rainrate area of the 1987 Valtellina storm are consistent. According to Table 2 and relevant to point (b) above, a few pixels with SSM/I estimates equal to zero are present in the region of the Meteosat-based high-rainrate areas, indicating that the IR scheme overestimates rain area. Note that most zero SSM/I rainrate pixels are concentrated in the low-rainrate areas.

6. Conclusions

Two heavy rainfall events associated with storms of different precipitation characteristics were studied using satellite-based IR and MW precipitation retrieval techniques (i.e. the NAWT and IFA-SAP algorithms). Among the results of the previous section, two are encouraging in pursuing a combined MW-IR approach for satellite heavy rainfall estimation:

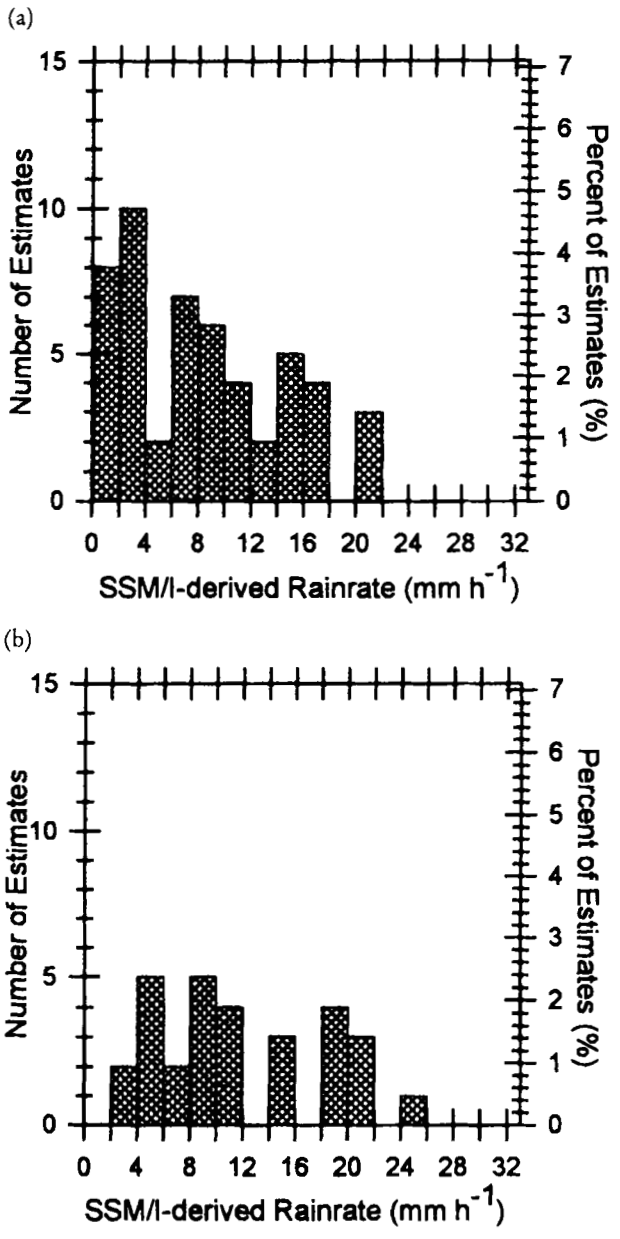

Figure 9. *Histograms of SSM/I-derived rainrate distribution for the 23 August 1987 event: pixels lying within Meteosat's (a) low-rainrate and (b) high-rainrate areas. Percentage values refer to the entire Meteosat-based precipitating area.*

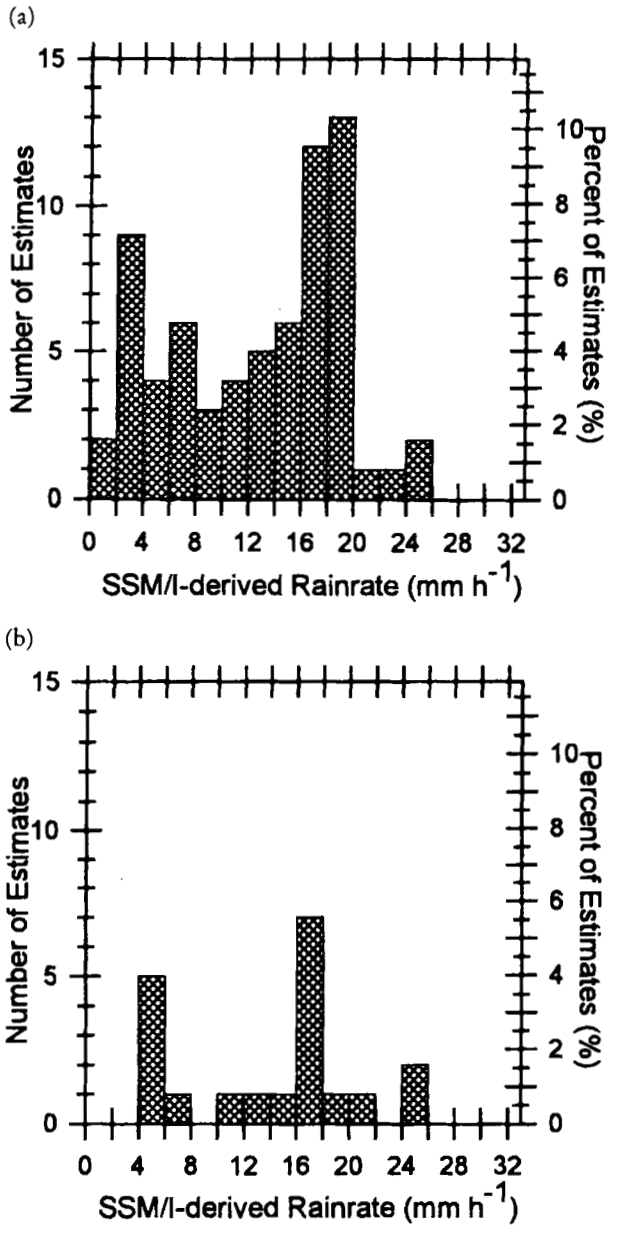

Figure 10. *Same as Fig. 9 but for the 27 September 1992 event.*

(a) Similarity between the rain areas has been found, particularly for the 1992 Genoa event.
(b) The mean values of SSM/I-derived precipitation within Meteosat's low-rainrate areas are consistently lower than those within Meteosat's high-rainrate areas.

The first result suggests that the NAWT-derived rain areas do not require re-calibration by the MW algorithm since the PCT screening used with the technique is effective in eliminating non-precipitating cold cloud areas. The second result suggests that the MW algorithm can be used as a calibration tool in the quantitative assignment of rainrate to the delimited rain areas, given that the NAWT's two rainrate thresholds are only nominally assigned and are not directly linked to the structure and composition of a specific storm.

Table 1. *Mean values of SSM/I rainrate estimates within Meteosat's low- and high-rainrate areas (mm h^{-1})*

	23 Aug. 1987	27 Sept. 1992
Low-rainrate	2.4	8.1
High-rainrate	9.9	14.0

The *Tropical Rainfall Measuring Mission* (TRMM) satellite to be launched in 1997 will provide simultaneous visible (VIS), IR, MW, and radar observations, thus ensuring an unprecedented multi-sensor and multi-

Table 2. *Number of SSM/I non-precipitating pixels within Meteosat's low- and high-rainrate areas. Percentage values refer to entire Meteosat precipitating area*

	23 Aug. 1987	27 Sept. 1992
Low-rainrate	126 (60%)	38 (30%)
High-rainrate	5 (2%)	0

channel capability for rainfall estimates (Simpson *et al.*, 1988). Unfortunately, this satellite will be placed in a low inclination, non-sun synchronous orbit (35 degrees) that will not provide coverage of the entire Mediterranean basin. At present, the only possibility of synthesising such a multi-sensor system is by combining measurements from different instruments on polar and geosynchronous satellites. This will be helpful in developing an effective strategy for instantaneous precipitation estimation from a combination of high resolution IR and low resolution MW measurements.

The procedure developed in the present study has not achieved operational readiness. However, the current results suggest an approach for multi-sensor retrieval that could be put into practice during the era of the *Multi-Frequency Imaging Microwave Radiometer* (MIMR), which will provide global coverage and will be direct-broadcast. Given the technological constraint of MW sensors being operated only on low-orbit spacecraft, it is unreasonable to presume that MW sensors alone can provide sufficient information for flood warning systems. The optical-infrared instruments on geostationary satellites are far more suited to obtaining data at the space–time resolutions concomitant with the inherent scales of precipitation. However, MW instruments are well suited as a calibration source for VIS-IR algorithms. It is thus worthwhile to proceed with the combined approach.

A statistically significant number of cases would have to be examined before a reliable combined MW-IR algorithm could be put into service as an information source for a flood warning system. Generating such a case-by-case climatology will be a major undertaking but one worth doing because even moderate improvement in the current Italian flood warning system could make significant inroads in mitigating the human and economic devastation associated with flash floods on the Mediterranean coast. Detailed mesoscale model simulations of these systems are also needed to link better the internal microphysical structures to satellite observations. The present study is viewed as a first step toward these goals.

Acknowledgements

This research has been supported by Agenzia Spaziale Italiana (ASI), Gruppo Nazionale per la Difesa dalle Catastrofi Idrogeologiche of Italy, Commission of European Communities (contract EV5V-CT92-0167) within research program Climatology and Natural Hazards of the EC-ENVIRONMENT Programme 1991–1994, and by National Aeronautics and Space Administration Grants NAGW-3970 and NAG5-2672. NATO Grant CG-890894 has contributed essential travel support. The SSM/I data were provided by NASA's WetNet Project under the direction of Dr James Dodge. Raingauge data were kindly made available by Servizio Idrografico of Lombardia Region of Italy, and by Istituto di Idraulica of the Universitá di Genova.

References

Adler, R. F., Negri, A. J., Keehn, P. R. & Hakkarinen, I. M. (1993). Estimation of monthly rainfall over Japan and surrounding waters from a combination of low-orbit microwave and geosynchronous IR data. *J. Appl. Meteorol.*, **32:** 335–356.

Allam, R., Holpin, G., Jackson, P. & Liberti, G. L. (1993). *Second Algorithm Intercomparison Project of the Global Precipitation Climatology Project: AIP-2.* Pre-Workshop Report, UKMO, Bracknell, Berkshire, UK, 133 pp.

Arkin, P. A. & Meisner, B. N. (1987). The relationship between large-scale convective rainfall and cold cloud over the western hemisphere during 1982–84. *Mon. Wea. Rev.*, **115:** 51–74.

Arkin, P. A. & Janowiak, J. (1991). Analysis of the global distribution of precipitation. *Dyn. Atmos. Oceans*, **16:** 5–16.

Barrett, E. C. & Michell, J. (1991). Satellite remote sensing of natural hazards and disasters in the Mediterranean region. In *Current Topics in Remote Sensing.* Vol. 2 (E. C. Barrett, K. A. Brown, & A. Michallef, editors), 51–67 Gordon & Breach.

Evans, K. F., Turk, J., Wong, T. & Stephens, G. (1995). A Bayesian approach to microwave precipitation profile retrieval. *J. Appl. Meteorol.*, **34:** 260–279.

Ferraro, R. R., Grody, N. C. & Marks, G. F. (1994). Effects of surface conditions on rain identification using the DMSP-SSM/I. *Rem. Sens. Rev.*, **11:** 195–210.

Grody, N. C. (1991). Classification of snow cover and precipitation using the Special Sensor Microwave Imager. *J. Geophys. Res.*, **96:** 7423–7435.

Kummerow, C. & Giglio, L. (1994). A passive microwave technique for estimating rainfall and vertical structure information from space. Part I: Algorithm description. *J. Appl. Meteorol.*, **33:** 3–18.

Levizzani, V., Porcú, F. & Prodi, F. (1990). Operational rainfall estimation using METEOSAT infrared imagery: an application in Italy's Arno river basin. Its potential and drawbacks. *ESA J.*, **14:** 313–323.

Levizzani, V., Mugnai, A., Porcú, F., Prodi, F., Smith, E. A. & Xiang, X. (1993). Comparison of rainfall estimates using SSM/I and METEOSAT measurements. In *IRS'92: Current Problems in Atmospheric Radiation* (S. Keevallik & O. Kärner, editors), 65–68. A. Deepak Publ., Hampton, VA.

Marrocu, M., Pompei, A., Dalu, G., Liberti, G. L. & Negri, A. J. (1993). Precipitation estimation over Sardinia from satellite infrared data. *Int. J. Remote Sensing*, **14:** 115–134.

Marzano, F. S., Mugnai, A., Smith, E. A., Xiang, X., Turk, J. & Vivekanandan, J. (1994). Active and passive remote sensing of precipitating storms during CaPE. Part II: Intercomparison of precipitation retrievals from AMPR radiometer and CP-2 radar. *Meteorol. Atmos. Phys.*, **54:** 29–51.

Mugnai, A., Cooper, H. J., Smith, E. A. & Tripoli, G. J. (1990). Simulation of microwave brightness temperatures of an evolving hailstorm at SSM/I frequencies. *Bull. Am. Meteorol. Soc.*, **71:** 2–13.

Mugnai, A., Cooper, H. J. & Tripoli, G. J. (1993). Foundations for statistical–physical precipitation retrieval from passive microwave satellite measurements. Part II: Emission source and generalized weighting-function properties of a time dependent cloud-radiation model. *J. Appl. Meteorol.*, **32:** 17–39.

Negri, A. J. & Adler, R. F. (1993). An intercomparison of three satellite infrared rainfall techniques over Japan and surrounding waters. *J. Appl. Meteorol.*, **32:** 357–373.

Negri, A. J., Adler, R. F. & Wetzel, P. J. (1984). Rain estimation from satellite: An examination of the Griffith–Woodley technique. *J. Appl. Meteorol.*, **23:** 102–116.

Petty, G. W. (1995). The status of satellite-based rainfall estimation over land. *Rem. Sens. Environ.*, **51:** 125–137.

Pierdicca, N., Marzano, F. S., D'Auria, G., Basili, P., Ciotti, P. & Mugnai, A. (1996). Precipitation retrieval from spaceborne microwave radiometers based on maximum a posteriori probability estimation. *IEEE Trans. Geosci. Rem. Sens.*, **34**, submitted.

Siccardi, F. (1987). Objectives of the National Group for the Prevention of Hydro-Geological Disasters. In *The Records of the Int. Conf. on the Arno Project* (I. Becchi & D. Giuli, editors). 3–7. CNR-GNDCI, No. 29.

Simpson, J., Adler, R. F. & North, J. (1988). A proposed Tropical Rainfall Monitoring Mission (TRMM) satellite. *Bull. Am. Meteorol. Soc*, **69:** 228–295.

Smith, E. A. & Mugnai, A. (1989). Radiative transfer to space through a precipitating cloud at multiple microwave frequencies. Part III: Influence of large ice particles. *J. Meteorol. Soc. Japan*, **67**: 739–755.

Smith, E. A., Mugnai, A., Cooper, H. J., Tripoli, G. J. & Xiang, X. (1992). Foundations for statistical–physical precipitation retrieval from passive microwave satellite measurements. Part I: Brightness temperature properties of a time dependent cloud-radiation model. *J. Appl. Meteorol.*, **31:** 506–531.

Smith, E. A., Xiang, X., Mugnai, A. & Tripoli, G. J. (1994). Design of an inversion-based precipitation profile retrieval algorithm using an explicit cloud model for initial guess microphysics. *Meteorol. Atmos. Phys.*, **54:** 53–78.

Smith, E. A., Chang, J. & Lamm, J. E. (1995). *Pip-2: Intercomparison Results Report.* Technical Document prepared under NASA WetNet Projects (NAGW-3970), Dept. of Meteorology, Florida State University, Tallahassee, FL, 38 pp., 7 appendices.

Smith, E. A., Mugnai, A. & Tripoli, G. (1996). Meteorological and climatic factors affecting extreme floods: prospects for prediction of terrain-forced events with a combination of mesoscale modeling and infrared-microwave precipitation retrieval. *Workshop Proceedings, United States–Italy Research Workshop on Hydrometeorology, Impacts, and Management of Extreme Floods* (November 13–17, Perugia, Italy), Water Resources Research and Documentation Center, Italian University for Foreigners, Perugia, Italy.

Spencer, R. W., Goodman, H. M. & Hood, R. E. (1989). Precipitation retrieval over land and ocean with SSM/I. Part I: Identification and characteristics of the scattering signal. *J. Atmos. Ocean. Technol.*, **6:** 254–273.

Tripoli, G. J. (1992). A nonhydrostatic model designed to simulate scale interaction. *Mon. Wea. Rev.*, **117:** 1342–1359.

Walter, L. (1986). Contribution of space technology to disaster preparedness, warning, and relief. In *Europe from Space* (O. Melita, editor), 103–107 European Space Agency-ESA SP-258, Paris.

Wilheit, T. T. (1986). Some comments on passive microwave measurement of rain. *Bull. Am. Meteorol. Soc.*, **67:** 1226–1232.

Wilheit, T. T., Adler, R. F., Avery, S., Barrett, E., Bauer, P., Berg, W., Chang, A., Ferriday, J., Grody, N., Goodman, S., Kidd, C., Kniveton, D., Kummerow, C., Mugnai, A., Olson, W., Petty, G., Shibata, A., Smith, E. A. & Spencer, R. (1994). Algorithms for the retrieval of rainfall from passive microwave measurements. *Rem. Sens. Rev.*, **11:** 163–194.